Discover Geoscience

RESEARCH Open Access

Seasonal variability in evapotranspiration partitioning in *Syngonium podophyllum* plant using dual stable isotopes (δ^2H and $\delta^{18}O$) at Roorkee, Uttarakhand

Gopal Krishan[1*], Anushka Chand[2*], Arif Ahamad[2], M. Someshwar Rao[1], Pravesh Singh[3], Diravia Balan[3], Richa Ojha[3], Rajesh Srivastava[3], Shivam Tripathi[3] and Saumyen Guha[3]

*Correspondence:
Gopal Krishan
drgopal.krishan@gmail.com
Anushka Chand
chandanushka83@gmail.com
[1]Hydrological Investigation Division, National Institute of Hydrology, Roorkee, Uttarakhand, India
[2]Jamia Millia Islamia University, New Delhi, India
[3]Department of Civil Engineering, Indian Institute of Technology Kanpur, Kanpur, India

Abstract

This study investigated the seasonal partitioning of evapotranspiration (ET) using dual stable isotopes (δ^2H and $\delta^{18}O$) for *Syngonium podophyllum* cultivated at the NIH Roorkee campus, Uttarakhand, India, during 2024. A total of 416 water samples were collected, comprising 93 soil evaporation, 82 leaf transpiration, 205 air moisture, and 36 rainfall samples, covering pre-monsoon, monsoon, post-monsoon, and winter seasons. Sampling was conducted every alternate day between 12:00–14:00 h to capture peak ET activity. The isotopic compositions of evapotranspiration (δ_{ET}), evaporation (δ_E), and transpiration (δ_T) were estimated using the Keeling Plot, Craig–Gordon, and steady-state models, respectively, and partitioned through a two-endmember isotopic mass balance approach. Results revealed pronounced seasonal variability in the transpiration fraction (T/ET) for *Syngonium podophyllum*, with mean values ranging from 0.52 during monsoon to 0.95 in post-monsoon, and an annual mean of 0.76 ± 0.15. Transpiration dominated total ET during the pre-monsoon (T/ET = 0.65–0.69), post-monsoon (0.93–0.95), and winter (0.84–0.89) seasons, while evaporation contributions increased substantially during the monsoon (0.51–0.54), coinciding with high soil moisture and rainfall events that suppressed transpiration. These findings demonstrate that transpiration by *Syngonium podophyllum* was the major component of ET for most of the year, except during the monsoon when direct soil evaporation prevailed. The results highlight how hydroclimatic variability regulates plant-scale water fluxes, and emphasize that irrigation management in humid subtropical regions should aim to minimize soil evaporation losses during wet periods and enhance transpiration efficiency during dry seasons. The isotope-based framework also provides a robust, non-invasive tool for quantifying plant–soil–atmosphere water exchanges.

Keywords Evapotranspiration, Isotopic technique, Evapotranspiration, Soil evaporation, Plant transpiration

© The Author(s) 2026. **Open Access** This article is licensed under a Creative Commons Attribution-NonCommercial-NoDerivatives 4.0 International License, which permits any non-commercial use, sharing, distribution and reproduction in any medium or format, as long as you give appropriate credit to the original author(s) and the source, provide a link to the Creative Commons licence, and indicate if you modified the licensed material. You do not have permission under this licence to share adapted material derived from this article or parts of it. The images or other third party material in this article are included in the article's Creative Commons licence, unless indicated otherwise in a credit line to the material. If material is not included in the article's Creative Commons licence and your intended use is not permitted by statutory regulation or exceeds the permitted use, you will need to obtain permission directly from the copyright holder. To view a copy of this licence, visit http://creativecommons.org/licenses/by-nc-nd/4.0/.

1 Introduction

The cumulative water transport from terrestrial surfaces to the atmosphere via soil evaporation (E) and plant transpiration (T) is referred to as evapotranspiration (ET), a key mechanism in the terrestrial hydrological cycle [1]. ET returns approximately 70–90% of terrestrial precipitation to the atmosphere and therefore plays a fundamental role in regulating ecosystem water balance, land–atmosphere interactions, and surface energy exchange.

It is essential to understand how ET is broken down into its component parts in order to evaluate ecosystem water use, improve agricultural management techniques, and increase water-use efficiency [2]. Because soil evaporation represents non-productive water loss whereas plant transpiration is directly linked to photosynthesis and biomass production, distinguishing these two components is essential for developing efficient water management strategies particularly in semi-arid agricultural environments, where the sustainability of irrigation strategies depends on the optimal distribution of water resources throughout various crop phenological stages, it is critical to accurately assess crop water requirements and analyse their temporal fluctuations [3].

Conventional techniques for evapotranspiration partitioning, such as sap flow measurements, lysimeter measurements, and micrometeorological methods, offer useful information, but often have limitations in terms of temporal resolution, spatial scalability, and the ability to non-invasively distinguish between transpiration and evaporation [4, 5]. Eddy covariance systems, although effective for measuring total ET, generally require additional assumptions or complementary observations to separate E and T, while hydrological models frequently depend on extensive parameterization and calibration that may introduce uncertainties in partitioning estimates. Recent advances in stable isotope techniques have opened up new avenues for evapotranspiration partitioning [4, 6, 7]. These methods are founded on isotope fractionation processes, whereby soil evaporation preferentially removes lighter isotopes, enriching the remaining soil water in heavier isotopes, whereas transpiration is generally considered a non-fractionating process during root water uptake under isotopic steady-state conditions. Consequently, the contrasting isotopic compositions of evaporation and transpiration provide a natural basis for quantifying their relative contributions to total ET.

The Global and Local Meteoric Water Lines (GMWL and LMWL) serve as fundamental reference systems in evapotranspiration (ET) partitioning by representing the isotopic composition of unaltered meteoric source waters. The theoretical basis for partitioning lies in the contrasting fractionation effects: abiotic soil evaporation (E) causes residual water to deviate and plot below the LMWL along a Soil Evaporation Line (SEL) with a significantly reduced slope, typically between 2.0 and 6.5. In contrast, plant transpiration (T) is generally assumed to be a non-fractionating process during root water uptake, meaning xylem water signatures remain relatively close to the LMWL.

High-resolution, non-invasive measurements of evaporation and transpiration in intact soil-plant-atmosphere systems are made possible by isotopic methods such as the Craig–Gordon model and the Keeling plot technique [8, 9].

Numerous factors, such as vegetation phenology, climatic variability, and soil moisture availability, influence the seasonal dynamics of ET partitioning [1, 10].Research has shown, for instance, that the temporal distribution of evaporation and transpiration affects yield and water use efficiency in winter wheat and maize, with some growth

stages responding better to optimal fertilisation or irrigation techniques [11]. Despite these advances, the relative contributions of soil evaporation and plant transpiration remain insufficiently quantified under varying seasonal and meteorological conditions, particularly for different plant species grown under humid subtropical environments.

Using stable isotope techniques, this study examines the seasonal variability of ET partitioning with an emphasis on the interaction between environmental factors. Our goal is to document the dynamic changes in the relative contributions of soil evaporation and plant transpiration by examining isotopic data gathered during significant phenological periods. Precision water management techniques in agricultural landscapes can be developed with the help of these insights, ultimately promoting resource conservation and sustainable crop production.

In view of this background, the specific objectives of this study are to partition the ET flux into soil evaporation (E) and plant transpiration (T) and investigate their seasonal fluctuations across selected plant species, as well as to assess the role of meteorological parameters in influencing ET dynamics. Based on prior evidence, we hypothesize that transpiration constitutes the dominant contributor to ET fluxes.

2 Materials and methods

2.1 Study area

The study was conducted at the National Institute of Hydrology (NIH), Roorkee (Uttarakhand), India (Fig. 1), which is located at an elevation of 268 m above mean sea level, at latitude 29°52′ N and longitude 77°53′ E. In the Roorkee region, the rice-wheat cropping system is the most common agricultural practice and the main source of income for the local populace. In addition to these staple commodities, farmers also grow sugarcane and other high-value crops. A combination of groundwater extraction and canal-based irrigation systems is the main source of water for the region's heavily irrigated agricultural areas [12]. This is a single experimental site; so for this results may not be generalized.

2.1.1 Meteorological conditions

Meteorological conditions exhibited clear seasonal patterns. Daily meteorological observations were obtained from the Automated Weather Station (AWS) of the National Institute of Hydrology (NIH), Roorkee. The station is equipped with standard meteorological sensors that continuously monitor atmospheric conditions and automatically record data at regular intervals. Rainfall was measured using an automatic rain gauge, while maximum and minimum air temperatures were recorded using electronic temperature sensors equivalent to standard maximum and minimum thermometers. Relative humidity was measured using capacitive humidity sensors providing continuous humidity records. Wind speed was measured using a cup anemometer, and wind direction was determined using a wind vane. Daily evaporation was measured using a standard Class A pan evaporimeter installed at the observatory. Daily values of maximum temperature, minimum temperature, relative humidity, rainfall, evaporation, wind speed, and wind direction were extracted from the AWS database and used for subsequent meteorological and isotopic analyses.

The study site receives an average annual rainfall of 953 mm, approximately 90% of which occurs during the southwest monsoon study area experiences a humid subtropical

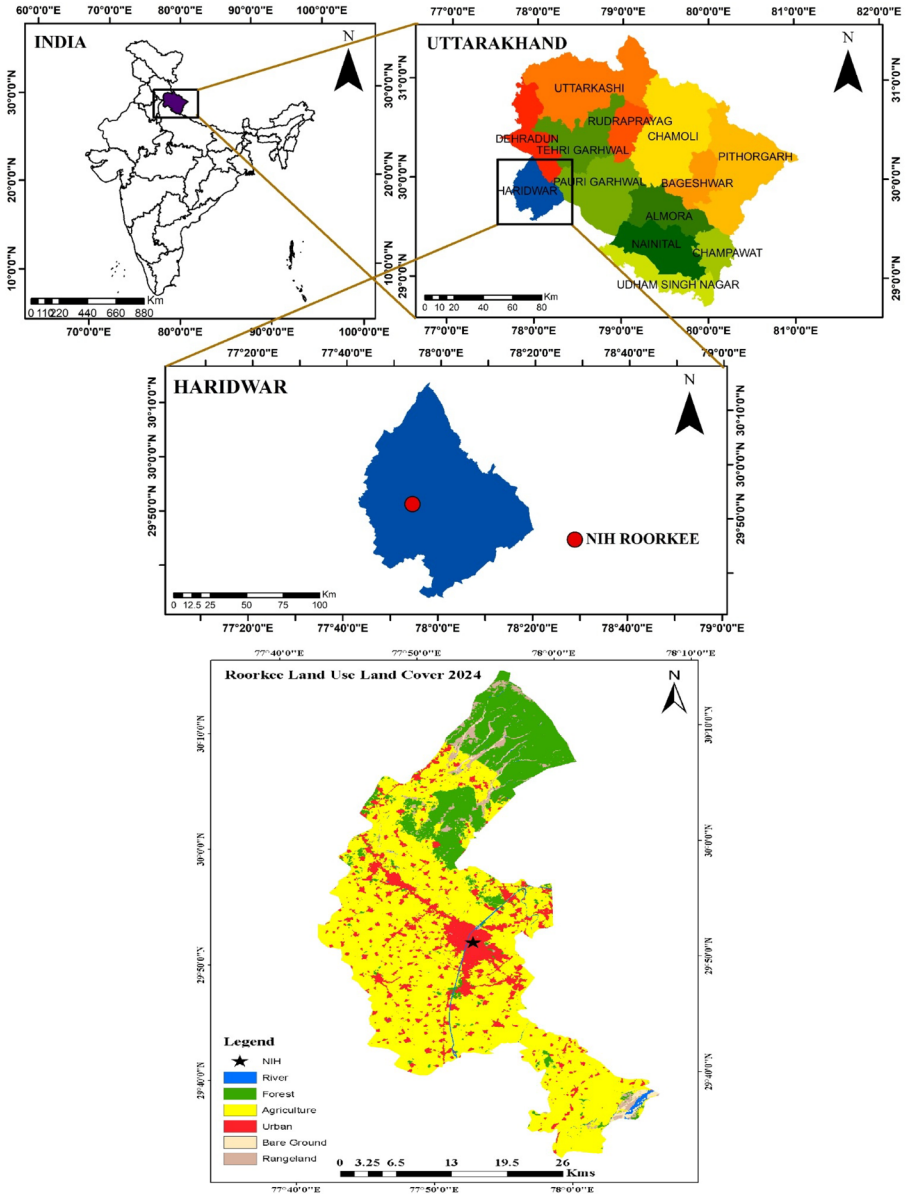


Fig. 1 Study area

climate characterized by distinct seasonal variations. The southwest monsoon extends from June to August, accounting for the major rainy season in the region. During the pre-monsoon period, the average maximum temperature was 34.2 °C, the minimum temperature 20.9 °C, precipitation 0.3 mm/day, evaporation 4.3 mm/day, relative humidity 69%, and wind speed 2.2 km/h. The monsoon season was characterised by maximum and minimum temperatures of 35.4 °C and 27.5 °C, respectively, with higher precipitation at 7.0 mm/day, evaporation at 4.0 mm/day, a relative humidity of 83%, and a wind speed of 1.6 km/h. After the monsoon, temperatures decreased to an average maximum of 27.7 °C and minimum of 16.1 °C, with precipitation at 0.2 mm/day, evaporation at 0.93 mm/day, relative humidity reaching 86.5%, and wind speed dropping to 0.42 km/h. In winter, conditions further cooled, showing average maximum and minimum temperatures of 18.6 °C and 9.5 °C, respectively. Precipitation remained low at 0.77 mm/

day, evaporation was 0.96 mm/day, relative humidity increased to 93.6%, and wind speed averaged 0.72 km/h. These seasonal meteorological variations are vital for understanding regional hydrological and isotopic processes.

2.2 Sample collection and isotopic analysis

Integrated sampling for air moisture, plant transpiration, soil evaporation, and rainwater was carried out to separate ET into its constituent parts, soil evaporation and plant transpiration and examine their temporal dynamics [7, 13]. The collection of each sample was done every alternate day between 12:00–14:00 h between all field days. Water flows throughout the soil, plant, and atmospheric continuum were traced by analysing all collected samples for stable isotopes (δ^2H and $\delta^{18}O$).

2.2.1 Air moisture sampling

A locally designed cone-condensation device was used to gather samples of atmospheric moisture. To collect condensate, a collecting vial was positioned beneath the apex of an aluminium cone fixed on a vertical stand. The setup was placed in an open area with good ventilation, away from any vegetation or bodies of water, and protected from direct sunlight. To reduce diurnal fluctuation and ensure comparable conditions, the samples were collected at the same place and time each day (during morning hours). The amount of collected condensate ranged from 5 to 10 ml, depending on the surrounding humidity. For isotopic analysis, the samples were promptly sealed and stored [12].

2.2.2 Plant transpiration sampling

Syngonium podophyllum is a fast-growing evergreen climbing vine with a C3 photosynthetic pathway, known for its broad, arrow-shaped leaves that change shape as the plant matures. It possesses a fibrous root system and exhibits relatively high transpiration rates under favourable environmental conditions, making it well suited for studies of plant water use. It adapts well to varying light and moisture conditions, making it useful for studying plant phenology and water use. Its distinct leaf morphology and root characteristics facilitate effective separation of transpiration and soil evaporation in evapotranspiration studies. The plant's sensitivity to environmental changes, rapid growth, and adaptability to the humid subtropical climate of the study area make it valuable for understanding water dynamics and plant responses in different ecosystems. Leaf-bag condensate collection for isotopic analysis of transpiration is a well-established, non-destructive method validated in multiple peer-reviewed studies [9, 14]. Polyethylene transpiration bags were sealed around leaf clusters of the plant during peak transpiration hours (12:00–14:00 h) to ensure high vapour flux and rapid condensation [14]. Condensate was collected in sterile glass vials placed inside the bags and immediately transferred to sealed vials for storage, minimising residence time and potential re-evaporation artefacts [15]. Individuals were maintained under natural field conditions at the study site, exposed to partial/filtered sunlight and sustained by ambient soil moisture from the region's canal- and groundwater-supported irrigation system, without direct irrigation applied by the research team. No fertilizers or pesticides were used during the sampling period to avoid confounding the isotopic measurements. The relative contributions of soil evaporation (E/ET) and plant transpiration (T/ET) to total evapotranspiration (ET) were estimated using isotopic values of δ_E, δ_T, and δ_{ET}. The assumption

of isotopic steady state was validated by ensuring that sampling was conducted during periods of high transpiration flux, when stomatal conductance and vapour flow rates are maximal [14]. Although sealed enclosures can potentially modify leaf microclimatic conditions such as temperature and humidity, several features of the experimental design minimised these effects. Ambient relative humidity at the Roorkee site remained consistently high, 69–93.6% across seasons and generally above 80% during monsoon and post-monsoon periods), reducing the vapour pressure gradient and limiting re-evaporation of condensate. In addition, relatively small polyethylene bags with limited headspace were used, allowing rapid condensation of freshly transpired vapour and minimising vapour residence time within the enclosure.

The Keeling Plot approach is widely used to estimate the isotopic composition of evapotranspiration by analysing the relationship between the isotopic ratio of atmospheric vapour and the inverse of its water vapour concentration, assuming that background conditions remain stable over short time intervals [16, 17]. This relationship is described by the equation: dynamics and plant responses in different ecosystems. With as little disruption to the leaves as possible, the bags were fastened and left in place until condensation took place. Sterile glass vials were used to collect the water droplets that formed inside the bags [16].

The Keeling Plot approach is widely used to estimate the isotopic composition of evapotranspiration (δ_{ET}) by analysing the relationship between the isotopic ratio of atmospheric vapour (q_v) and the inverse of its water vapour concentration, assuming background conditions remain stable over short time intervals [18]. This relationship is described by the equation:

$$\delta_V = \delta_E T + (\delta_B - \delta_E T) \times (q_B / q_V) \quad (1)$$

where δ_v is the isotopic composition of ambient atmospheric water vapor and q_v is the concentration of atmospheric water vapour. δ_B and q_B refer to the background vapour's isotopic composition and concentration, respectively. By plotting δ_v against $1/q_v$, the y-intercept of the linear regression provides an estimate of δ_{ET} [19, 20]. This method assumes that δ_B, q_B and δ_{ET}remain constant during the sampling period, and that water vapour is transported solely by turbulent mixing, without influence from condensation or other processes.

2.2.3 Soil evaporation sampling

A transparent acrylic box of 75 × 75 × 60 cm was used to create an experimental evaporation chamber that stimulates soil evaporation in a natural field setting [18]. Through the use of pipelines and valves, the system's air compressor was able to draw water vapour from the soil's surface and transfer it to a condensation unit submerged in ice water. Airflow was managed by a rotameter and nozzle valve, while humidity gradients within and outside the chamber were recorded by a relative humidity meter. The assumption of isotopic steady state was validated by ensuring that sampling was conducted during periods of high transpiration flux. Soil water vapour was sampled directly from the evaporating front of the soil using a chamber-based experimental setup installed at the study site. This approach allowed us to capture the isotopic signature of soil evaporation (E) in real-time without disturbing the natural evaporation process. The Craig-Gordon model was applied to estimate the isotopic composition of vapour evaporating from the soil surface.

This method accounts for both equilibrium and kinetic fractionation processes and is appropriate under steady-state conditions. Using measured values of soil water, ambient vapour, relative humidity, and temperature, the model yielded dependable estimates of isotopic enrichment due to evaporation in the controlled chamber environment.

The Craig and Gordon model is used to estimate the isotopic composition of soil evaporation (δ_E), considering both equilibrium and kinetic isotope fractionation during water vapour diffusion from the soil surface [21]. In this model, δ_E is affected by the isotopic signature of soil water at the evaporating front (δ_L), the isotopic composition of ambient atmospheric vapour (δ_v), as well as temperature and relative humidity. The following equation is applied:

$$\delta_E = \frac{\delta_L\left(\frac{1}{\alpha_{eq}}\right) - h\delta_v - \varepsilon_{eq} - (1-h)\varepsilon_k}{(1-h) + 10^{-3}(1-h)\varepsilon_k} \quad (2)$$

where δ_L is the isotopic composition of soil water at the evaporating front, δ_v is the isotopic composition of ambient atmospheric water vapor, h is the relative humidity normalized to saturation vapor pressure at the soil surface temperature (dimensionless, 0–1), α_{eq} is the temperature-dependent equilibrium fractionation factor for liquid-vapor phase transition, ϵ_{eq} is the equilibrium enrichment factor in delta notation, and ϵ_k is the kinetic fractionation factor representing non-equilibrium effects during vapor diffusion [22].

The equilibrium fractionation factor α_{eq} was calculated as a function of soil surface temperature using the temperature-dependent relationship established by Horita and Wesolowski [23].The equilibrium enrichment factor ϵ_{eq} was derived from α_{eq}using the equation $\varepsilon_{eq} = 10^3\left(1 - \frac{1}{\alpha_{eq}}\right)$. The kinetic fractionation factor ϵ_k was determined using the molecular diffusivity ratio approach $\varepsilon_k = n\left(\frac{D}{D_i} - 1\right) \times 10^3$, where D/Di is the ratio of molecular diffusivities of the light to heavy isotope (1.0285 for ^{18}O and 1.0251 for ^{2}H), and n is the turbulence parameter ranging from 0 (fully turbulent conditions) to 1 (purely molecular diffusion). Based on the controlled chamber conditions with minimal air circulation, an n value of 0.5 was adopted, yielding ϵ_k values of 14.2‰ for $\delta^{18}O$ and 12.5‰ for $\delta^{2}H$ [24].

2.2.4 Isotopic analysis

At National Institute of Hydrology, isotope ratio mass spectrometry (IRMS) was used to examine all water samples for $\delta^{2}H$ and $\delta^{18}O$. Delta notation (δ) in relation to VSMOW standards was used to report the results [25]. For $\delta^{18}O$ and $\delta^{2}H$, the analytical precision was ± 0.1‰ and ± 1‰, respectively. To ensure accuracy, calibration was carried out utilizing secondary standards and three-point standardization with international reference materials (VSMOW, GISP, SLAP). Quality control samples were included in every analytical run, and chosen samples were examined in duplicate to confirm reproducibility [12].

2.3 Isotope partitioning approach

The proportion of evapotranspiration (T/ET) originating from transpiration is determined using a two-source linear mixing model that incorporates the isotopic

compositions of evapotranspiration (δ_{ET}), evaporation (δ_E), and transpiration (δ_T). The equation for this calculation is:

$$T/ET = \frac{\delta_{ET} - \delta_E}{\delta_T - \delta_E} \tag{3}$$

This method is based on an isotopic mass balance equation, where the total ET flux is composed of the contributions from both evaporation and transpiration, each characterized by unique isotopic signatures [26]. By analysing the isotopic compositions of water vapor, soil, and plant xylem, the fluxes are separated into their respective components [16].

2.4 Uncertainty quantification and error propagation

2.4.1 Analytical error propagation

Analytical uncertainties were propagated through Eq. 3 using standard error propagation theory to quantify the uncertainty in T/ET estimates arising from measurement precision:

$$\sigma^2(T/ET) = (\partial f/\partial \delta_E T)^2 \sigma^2(\delta_E T) + (\partial f/\partial \delta_E)^2 \sigma^2(\delta_E) + (\partial f/\partial \delta_T)^2 \sigma^2(\delta_T) \tag{4}$$

where the partial derivatives are:

$$\frac{\partial f}{\partial \delta_{ET}} = \frac{1}{\delta_T - \delta_E} \tag{5}$$

$$\frac{\partial f}{\partial \delta_E} = \frac{(\delta_{ET} - \delta_T)}{(\delta_T - \delta_E)^2} \tag{6}$$

$$\frac{\partial f}{\partial \delta_T} = -\frac{(\delta_{ET} - \delta_E)}{(\delta_T - \delta_E)^2} \tag{7}$$

This yielded sample-specific analytical uncertainties of ± 0.19–0.21 for individual T/ET estimates. An additional model uncertainty of ± 0.05 was incorporated to account for assumptions in the mass balance approach (isotopic steady-state, negligible fractionation during vapor transport), resulting in combined analytical uncertainties of ± 0.19–0.21 for individual samples [10].

2.4.2 Combined uncertainty for seasonal means

Seasonal mean values and standard errors combined both analytical and sampling uncertainties according to:

$$SE_{combined} = \sqrt{SE_{sampling}^2 + SE_{analytical}^2} \tag{8}$$

where $SE_{sampling} = \frac{SD}{\sqrt{n}}$ represents natural temporal variability and $SE_{analytical} = \frac{\sigma_{analytical}}{\sqrt{n}}$ represents the contribution of measurement precision to seasonal mean uncertainty. This approach accounts for both random measurement error and systematic natural variability, providing realistic uncertainty bounds for seasonal T/ET estimates [27].

2.4.3 Monte carlo simulation and sensitivity analysis

Monte Carlo simulations (10,000 iterations) were performed to validate analytical error propagation calculations and generate 95% prediction intervals for T/ET estimates. For each iteration, input parameters ($\delta_{ET}, \delta_E, \delta_T$) were randomly sampled from normal distributions defined by their measured seasonal mean values and analytical uncertainties (± 0.2‰ for $\delta^{18}O$, ± 1.0‰ for δ^2H), and T/ET was recalculated using Eq. 3.

Sensitivity analysis employed standardized multiple linear regression on Monte Carlo output to quantify the relative contribution of each input parameter to total T/ET uncertainty. Input variables were standardized (mean-centerer and scaled by standard deviation), and T/ET outputs were similarly standardized. Standardized regression coefficients ($\beta_{standardized}$) were calculated and converted to percentage contributions by normalizing their absolute values to sum to 100%. This approach identifies which isotopic measurements contribute most to T/ET uncertainty, guiding priorities for improving analytical precision [28].

2.5 Statistical analysis

2.5.1 Analysis of variance (ANOVA)

Seasonal differences in isotopic composition and T/ET ratios were evaluated using one-way analysis of variance (ANOVA) with season as the independent variable (four levels: pre-monsoon, monsoon, post-monsoon, winter). Prior to ANOVA, assumptions of normality and homogeneity of variance were verified using Shapiro-Wilk tests (per seasonal group) and Levene's test (across all groups), respectively. All tests were conducted at significance level $\alpha = 0.05$.

Effect sizes were quantified using eta-squared (η^2) calculated as:

$$\eta^2 = \frac{SS_{between}}{SS_{total}} \tag{9}$$

where $SS_{between}$ is the sum of squares between groups and SS_{total} is the total sum of squares. Effect sizes of $\eta^2 > 0.01$, 0.06, and 0.14 were interpreted as small, medium, and large effects, respectively [29].

2.5.2 Post-hoc pairwise comparisons

Following significant ANOVA results ($p < 0.05$), post-hoc pairwise comparisons were conducted using Tukey's Honestly Significant Difference (HSD) test to control family-wise error rate at $\alpha = 0.05$. Additional pairwise t-tests with Bonferroni correction (adjusted $\alpha = 0.05/k$, where k is the number of comparisons) were performed for key seasonal contrasts [30].

For each pairwise comparison, Cohen's d effect size was calculated as:

$$d = \frac{M_1 - M_2}{SD_{pooled}} \tag{10}$$

where M_1 and M_2 are group means and $SD_{pooled} = \sqrt{\frac{SD_1^2 + SD_2^2}{2}}$ is the pooled standard deviation. Effect sizes of $d > 0.2$, 0.5, and 0.8 were interpreted as small, medium, and large, respectively.

2.5.3 Confidence intervals (CI)

Seasonal mean values are reported with 95% confidence intervals calculated using Student's t-distribution:

$$95\%CI = mean \pm t_{(\alpha/2,df)} \times SE_{combined} \quad (11)$$

where t(α/2, df) is the critical t-value for α = 0.05 and degrees of freedom df = n-1. Combined standard errors ($SE_{combined}$) incorporate both analytical precision and sampling variability [31].

2.5.4 Statistical power analysis

Post-hoc statistical power was evaluated for all ANOVA tests using the F-test power analysis function with observed effect sizes (η^2), sample sizes, and α = 0.05. Power values > 0.80 were considered adequate for reliable detection of true effects. All statistical analyses were performed using Python 3.11 with scipy.stats (version 1.11.3) and statsmodels (version 0.14.0) packages [30].

3 Results and discussion

3.1 Isotopic compositions of ecohydrological pools

A comparative assessment of stable isotope compositions across various ecohydrological pools reveals both temporal consistency and interannual variation shaped by climatic and hydrological processes (Fig. 2). The observed steepening of the Local Meteoric Water Line (LMWL) from 2023 to 2024, while remaining below the Global Meteoric Water Line (GMWL), aligns with Indian precipitation studies that report regional LMWL slopes commonly < 8 due to sub-cloud evaporation and recycled moisture, with documented slope ranges from roughly 6.9 to 8.8 across stations and seasons [32]. Multi-year rainfall datasets indicate $\delta^{18}O$ values typically spanning from − 18‰ to 2‰ and $\delta^{2}H$ values from − 130‰ to + 16‰, with modest interannual changes in meteoric line parameters, supporting the use of precipitation as a stable isotopic baseline [33].

Leaf water enrichment relative to the LMWL and the shallow $\delta^{2}H$–$\delta^{18}O$ slopes observed here are consistent with Craig–Gordon model expectations under low humidity conditions. Previous synthesis and field analyses similarly report that leaf and soil regression slopes are "much smaller" than the LMWL and highly sensitive to relative humidity and vapor pressure deficit [34].

Soil water samples generally follow low-slope evaporation lines, indicative of near-surface evaporative enrichment. Studies report slopes between approximately 3 and 6, including a cold-region relation ($\delta^{2}H = 3.23\ \delta^{18}O - 32.51$), which provides a numerical comparator for evaporated shallow soil layers [35].

Atmospheric vapor typically remains the most isotopically depleted component and exhibits slopes intermediate between soil and leaf water, reflecting the mixing of locally evaporated vapor with advected air masses.

3.2 Isotopic partitioning of ET

3.2.1 Evapotranspiration Isotopic Composition (δ_{ET}) from keeling plot analysis

To estimate δ_{ET}, linear regressions were applied using $\delta^{2}H$ of δ_{v} which is the isotopic composition of ambient atmospheric water vapor and q_{v} is the concentration of atmospheric water vapour concentration. Although both $\delta^{2}H$ and $\delta^{18}O$ were determined,

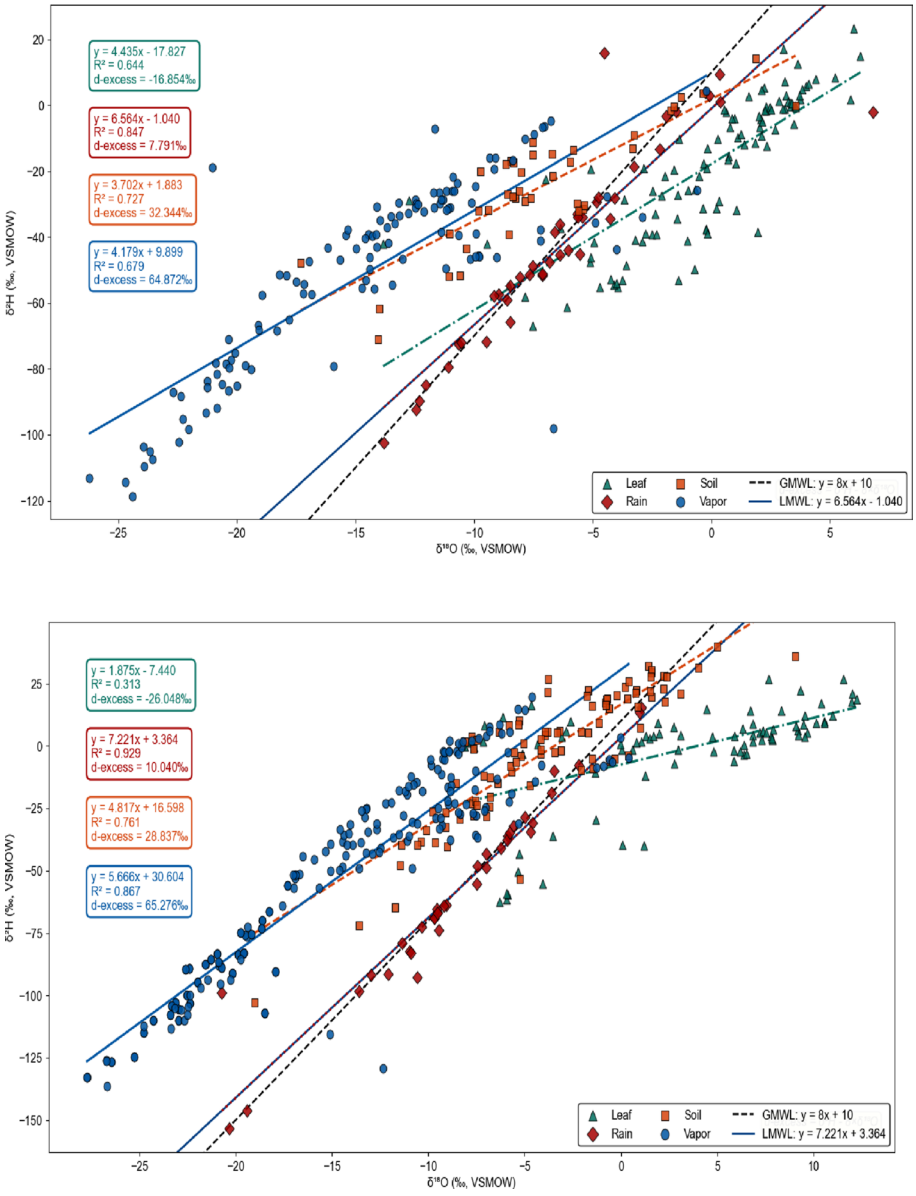


Fig. 2 δ^2H - $\delta^{18}O$ relationship for the water samples and the local meteoric water line (LMWL) in the (a) 2023 and (b) 2024

only δ^2H showed high statistical significance compared to $\delta^{18}O$ in the regression analysis, consistent with previous findings, which is why δ^2H is widely used for ET partitioning. The statistical results of the Keeling plot analysis with δ^2H are presented in Table 1 presents the δ^2H regression lines corresponding to the various sampling months. Seasonal regressions exhibited clear intra-annual structure in both slope and intercept parameters. Slopes were smallest in winter (December–January) with the least negative intercepts, indicating minimal kinetic enrichment under cool, stable conditions. From late winter into pre-monsoon (February–April), slopes increased and intercepts became more negative, consistent with growing evaporative influence prior to monsoon onset. The monsoon onset (June) showed the highest slopes alongside the largest standard errors, reflecting rapid hydroclimatic transitions; intercepts were strongly negative, indicative of enhanced kinetic effects and shifting moisture sources. During

Table 1 Regression analysis of the keeling plot of the collected vapour

Season	Month	Isotope	Slope (±SD)[a]	Intercept (±SD) [a]	R^2	*n*	*P*-value*
Winter	December	δ^2H	19.67 ± 4.93	-41.82 ± 4.62	0.550	15	0.001*
	January	δ^2H	1.56 ± 33.18	-21.42 ± 12.58	0.00074	5	0.965
	February	δ^2H	18.59 ± 45.94	-23.01 ± 30.17	0.0266	8	0.699
Pre-monsoon	March	δ^2H	51.48 ± 6.26	-52.82 ± 4.16	0.722	28	1.06e − 08*
	April	δ^2H	43.11 ± 7.53	-52.59 ± 4.16	0.731	14	9.58e − 05*
	May	δ^2H	24.31 ± 10.43	-45.74 ± 4.38	0.404	10	0.048*
Monsoon	June	δ^2H	109.60 ± 50.87	-123.76 ± 29.46	0.436	8	0.074*
	July	δ^2H	30.84 ± 7.99	-97.51 ± 4.07	0.650	10	0.004*
	August	δ^2H	36.23 ± 8.64	-119.58 ± 5.09	0.661	11	0.002*
	September	δ^2H	46.97 ± 11.12	-129.11 ± 6.85	0.597	14	0.001*
Post-monsoon	October	δ^2H	47.85 ± 7.17	-79.32 ± 4.36	0.689	22	1.71e − 06*
	November	δ^2H	19.31 ± 5.74	-54.51 ± 4.91	0.255	13	0.006*
	December	δ^2H	19.67 ± 4.93	-41.82 ± 4.62	0.550	15	0.001*

[a]Slope and intercept values are derived from the linear regression of δ^2H of δ_v versus the inverse of water vapor concentration q_v; ±SD denotes standard deviation

* $p < 0.05$ indicates statistically significant result

Table 2 Estimates of the isotopic composition (δ_T, δ_E, δ_{ET}) and the corresponding fractions of transpiration (T/ET) during different hydrological seasons (Pre-monsoon, Monsoon, Post-monsoon and Winter)

Season	Month	δ_L	δ_v	δ_E	δ_{ET}	δ_T	T/ET
Pre-monsoon	March	-9.5	-9.11	-127.01	-52.82	-11.8	0.643
	April	-23.15	-29.89	-132.39	-52.59	-7.20	0.692
	May	-20.7	-35.25	-127.18	-45.74	-3.60	0.658
Monsoon	August	-64	-100.34	-180.27	-119.59	-62.49	0.515
	September	-102.74	-105.369	-207.77	-129.11	-62	0.539
Post-monsoon	October	-46.46	-59.39	-147.04	-79.31	-74.3	0.931
	November	-34	-38.76	-145.36	-54.51	-50	0.952
Winter	January	-10.31	-19.88	-117.78	-21.4	-3.18	0.841
	February	-9.5	-12.46	-123.9	-23	-10.64	0.890

the monsoon core (July–August), slopes remained elevated with improved precision, and intercepts stayed strongly negative, pointing to sustained enrichment signals. Post-monsoon (September–November) parameters moderated toward winter baselines, with intermediate slopes and less negative intercepts, aligning with reduced evaporative demand and stabilization of background vapor.

3.2.2 Determination of T/ET

The seasonal and monthly distribution of ET components is presented in Table 2. During the pre-monsoon season (March to May), transpiration dominated the total ET, with T/ET values ranging from 0.643 to 0.692. These elevated values highlight the importance of plant water uptake during the dry months, as also observed in similar isotopic partitioning studies [36]. In contrast, the monsoon period (August and September) exhibited a decline in T/ET values (0.515 and 0.539, respectively), indicating a greater contribution of soil evaporation. This shift corresponds with high precipitation levels and saturated soil conditions, which tend to suppress transpiration while enhancing evaporation rates. Following the monsoon, the post-monsoon period (October and November) showed a substantial rebound in transpiration dominance, with T/ET values increasing to 0.931 and 0.952. This is likely due to reduced rainfall, improved soil drainage, and active plant

recovery post-rainy season. The winter season (January and February) sustained high T/ET values (0.841 and 0.890), reaffirming that transpiration remains the principal component of ET during cooler months, consistent with previous findings in temperate and subtropical climates [37]. These results collectively demonstrate a seasonal pattern of ET partitioning, where transpiration predominates during dry and cold months, while evaporation gains prominence during wet periods, reflecting shifts in plant physiological activity and hydrological availability (Table 3).

3.3 Seasonal variation in evapotranspiration isotopes

The isotopic composition of evapotranspiration (δ_{ET}) showed strong and significant seasonal differences across pre-monsoon, monsoon, post-monsoon, and winter periods, with season explaining 96.7% of the variance (ANOVA: $F(3,5) = 48.95$, $p = 0.0004$, $\eta^2 = 0.967$; Fig. 3; Table 4). Mean δ_{ET} was most depleted during monsoon (– 124.35‰, 95% CI: –185.50, – 63.20‰), intermediate in post-monsoon (– 66.91‰, 95% CI: –224.72, 90.90‰), and enriched during winter (– 22.20‰, 95% CI: –35.77, – 8.63‰), while pre-monsoon occupied an intermediate enriched state (– 50.38‰, 95% CI: –60.68, – 40.09‰) (Fig. 3; Table 3). Tukey HSD indicated monsoon was significantly more depleted than pre-monsoon (mean difference = 73.97‰, $p = 0.001$), post-monsoon (57.44‰, $p = 0.0048$), and winter (102.15‰, $p = 0.0003$), reflecting the seasonal "amount effect" on precipitation and enhanced exchange with moist boundary layers during the wet season (Fig. 3; Table 5).

The isotopic composition of soil evaporation (δ_E) also varied significantly by season (ANOVA: $F(3,5) = 27.01$, $p = 0.0016$, $\eta^2 = 0.942$; Fig. 4; Table 4). Monsoon exhibited the most depleted soil vapor (– 194.02‰, 95% CI: –368.96, – 19.08‰), followed by post-monsoon (– 146.20‰, 95% CI: –160.15, – 132.25‰), pre-monsoon (– 128.86‰, 95% CI: –136.85, – 120.87‰), and winter (– 120.84‰, 95% CI: –160.75, – 80.93‰) (Fig. 4; Table 3). Monsoon differed significantly from pre-monsoon ($\Delta = 65.16$‰, $p = 0.0021$), post-monsoon (47.82‰, $p = 0.0125$), and winter (73.18‰, $p = 0.0019$), indicating stronger evaporative depletion under wetter surface conditions and reduced vapor pressure deficit (Fig. 4; Table 5).

Assumptions diagnostics indicated near-normal seasonal groups (e.g., Shapiro-Wilk pre-monsoon $p > 0.05$) but heterogeneous variances for δ_{ET} and δ_E (Levene's $p = 0.018$ and 0.003, respectively.

3.4 Evapotranspiration partitioning (T/ET)

T/ET ratios exhibited pronounced seasonal structure with very large effect size (ANOVA: $F(3,5) = 123.82$, $p < 0.0001$, $\eta^2 = 0.987$; Fig. 5; Table 4). Seasonal means (± 95% CI) were: pre-monsoon 0.65 (0.44, 0.89), monsoon 0.53 (– 0.13, 1.18), post-monsoon 0.94 (0.29, 1.59), and winter 0.87 (0.16, 1.57), indicating transpiration dominance during dry and cool periods and enhanced evaporation during monsoon (Fig. 5; Table 3). Tukey comparisons showed the largest contrast between monsoon and post-monsoon ($\Delta = 0.414$, $p = 0.0001$), followed by monsoon vs. winter (0.339, $p = 0.0001$) and monsoon vs. pre-monsoon (0.137, $p = 0.0061$), while post-monsoon vs. winter was not significant at $\alpha = 0.05$ ($\Delta = 0.076$, $p = 0.0896$) (Fig. 5; Table 5).

Table 3 Seasonal means ± 95% CI for δ_{ET}, δ_{E}, δ_{v}, δ_{T}, T/ET

Parameter	Pre-monsoon	Monsoon	Post-monsoon	Winter
δ_{ET}(‰)	−50.38 (− 60.68, − 40.09)	−124.35 (− 185.50, − 63.20)	−66.91 (− 224.72, 90.90)	−22.20 (− 35.77, − 8.63)
δ_{E}(‰)	−128.86 (− 136.85, − 120.87)	−194.02 (− 368.96, − 19.08)	−146.20 (− 160.15, − 132.25)	−120.84 (− 160.75, − 80.93)
δ_{v}(‰)	−24.75 (− 59.14, 9.64)	−102.85 (− 136.04, − 69.67)	−49.08 (− 180.45, 82.30)	−16.17 (− 64.16, 31.82)
δ_{T}(‰)	−7.53 (− 18.04, 2.97)	−62.25 (− 71.75, − 52.74)	−62.15 (− 216.79, 92.49)	−6.91 (− 55.15, 41.33)
T/ET	0.66 (0.44, 0.89)	0.53 (− 0.13, 1.18)	0.94 (0.29, 1.59)	0.87 (0.16, 1.57)

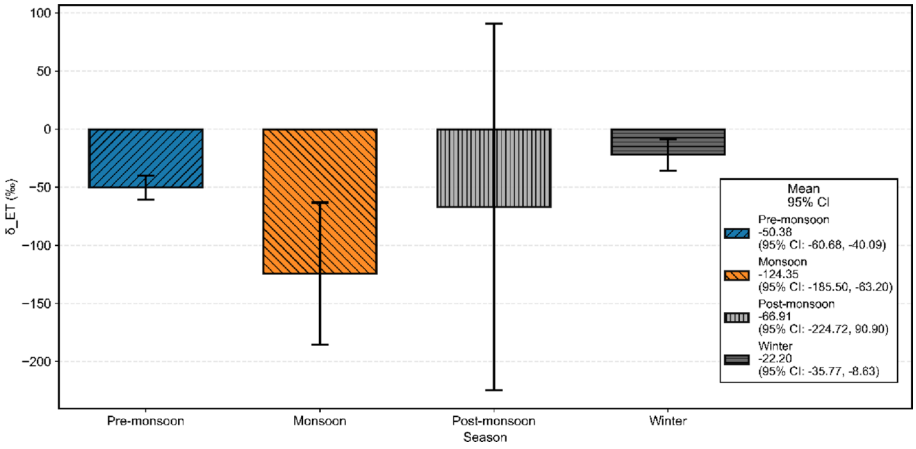


Fig. 3 Seasonal δ_{ET} with 95% CI

Table 4 Monte Carlo means, SD, 95% PI, and sensitivity weights

Parameter	F-statistic	Df	*p*-value	Significance	η^2	Power
δ_{ET} (‰)	48.95	(3, 5)	0.0004	***	0.967	1
δ_{E} (‰)	27.01	(3, 5)	0.0016	**	0.942	1
δ_{V} (‰)	25.27	(3, 5)	0.0019	**	0.938	1
δ_{T} (‰)	31.29	(3, 5)	0.0012	**	0.949	1
T/ET ratio	123.82	(3, 5)	0.0000	***	0.987	1

Table 5 Tukey HSD and pairwise t-tests with Cohen's d

Parameter	Comparison	Difference	CI (Lower)	CI (Upper)	T	*P*	Cohen's d	Significance
δ_{ET}	Pre-monsoon vs. Monsoon	73.97	63.59	84.35	15.92	0.00054	13.34	***
δ_{ET}	Monsoon vs. Post-monsoon	−57.44	−83.47	−31.41	−4.32	0.04953	−4.32	*
δ_{ET}	Post-monsoon vs. Winter	−44.71	−69.06	−20.36	−3.60	0.06931	−3.60	Ns
δ_{ET}	Pre-monsoon vs. Winter	-28.1833	-32.9981	-23.3685	-9.21868	0.0027	-9.53762	**
T/ET	Pre-monsoon vs. Monsoon	0.137333	0.10045	0.174216	6.621376	0.007016	6.409008	**
T/ET	Monsoon vs. Post-monsoon	-0.4145	-0.44575	-0.38325	-25.9953	0.001477	-25.9953	**
T/ET	Post-monsoon vs. Winter	0.076	0.023756	0.128244	2.851225	0.104145	2.851225	Ns
T/ET	Pre-monsoon vs. Winter	-0.20117	-0.25696	-0.14537	-7.69373	0.004563	-6.64885	**

3.5 Uncertainty quantification and Monte Carlo validation

Analytical uncertainty propagated through the mass-balance equation yielded small sample-level errors for T/ET (± 0.002–0.004), and Monte Carlo simulations (10,000 iterations) produced narrow seasonal 95% prediction intervals consistent with the analytical error budget: pre-monsoon [0.643, 0.651], monsoon [0.525, 0.532], post-monsoon [0.937, 0.950], and winter [0.861, 0.870] (Fig. 6; Table 6). Sensitivity analysis on the Monte Carlo ensemble showed δ_{ET} contributes the largest share of variance to T/ET (= 50%), followed by δ_{T} (= 27–47%) and δ_{E} (= 3–24%), implying efforts to further

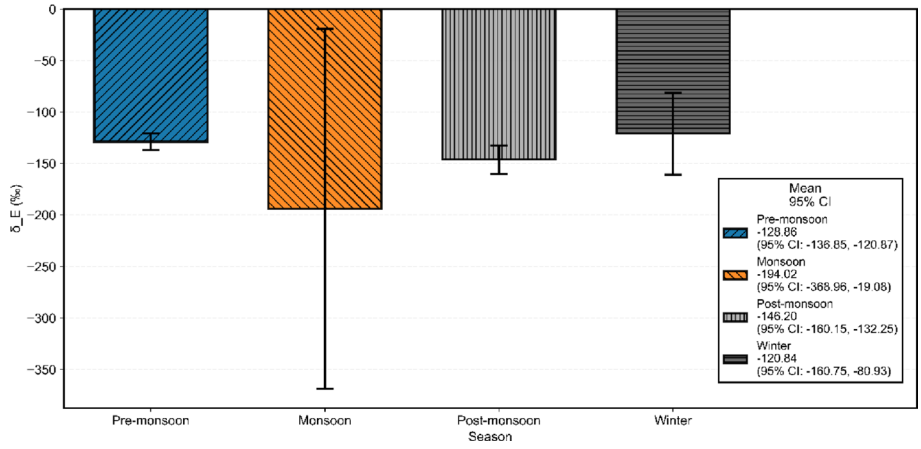


Fig. 4 Seasonal δ_E with 95% CI

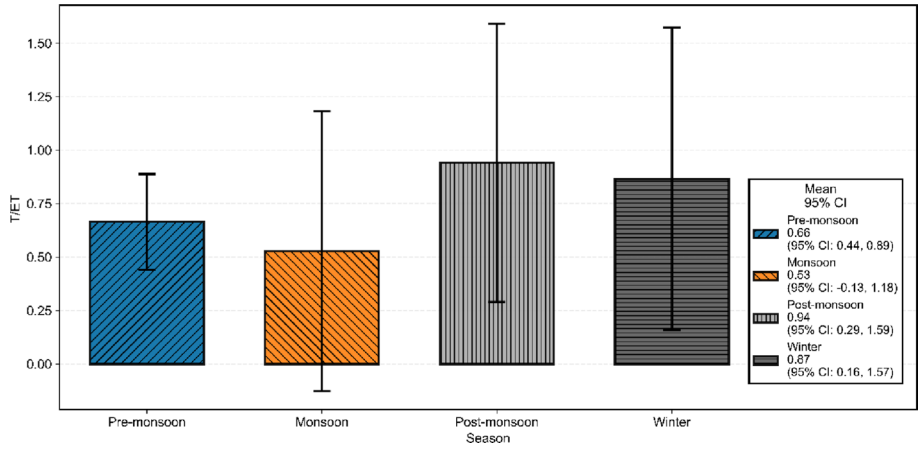


Fig. 5 Seasonal T/ET with 95% CI

reduce uncertainty should prioritize the precision of δ_{ET} and δ_T measurements (Fig. 6; Table 6).

3.6 Statistical power and robustness

Observed effect sizes were very large for all parameters (η^2 = 0.938–0.987), yielding post-hoc statistical power = 1.000 for all ANOVA tests (Table 4). Although Levene's tests indicated heteroscedasticity for δ_{ET} and δ_E, results were robust to Welch ANOVA and pairwise contrasts remained consistent in sign and magnitude (Table 5). Together, these results support strong, seasonally driven shifts in isotopic composition and evapotranspiration partitioning that exceed analytical and sampling uncertainties (Fig. 7).

3.7 Meteorological parameters influencing evapotranspiration ratio (T/ET)

The correlation matrix indicates that T/ET is negatively related to most meteorological drivers, with the largest magnitudes for rainfall and minimum temperature, while relative humidity shows a weak-to-moderate positive association, aligning with established controls of atmospheric demand and moisture constraints on evapotranspiration processes.

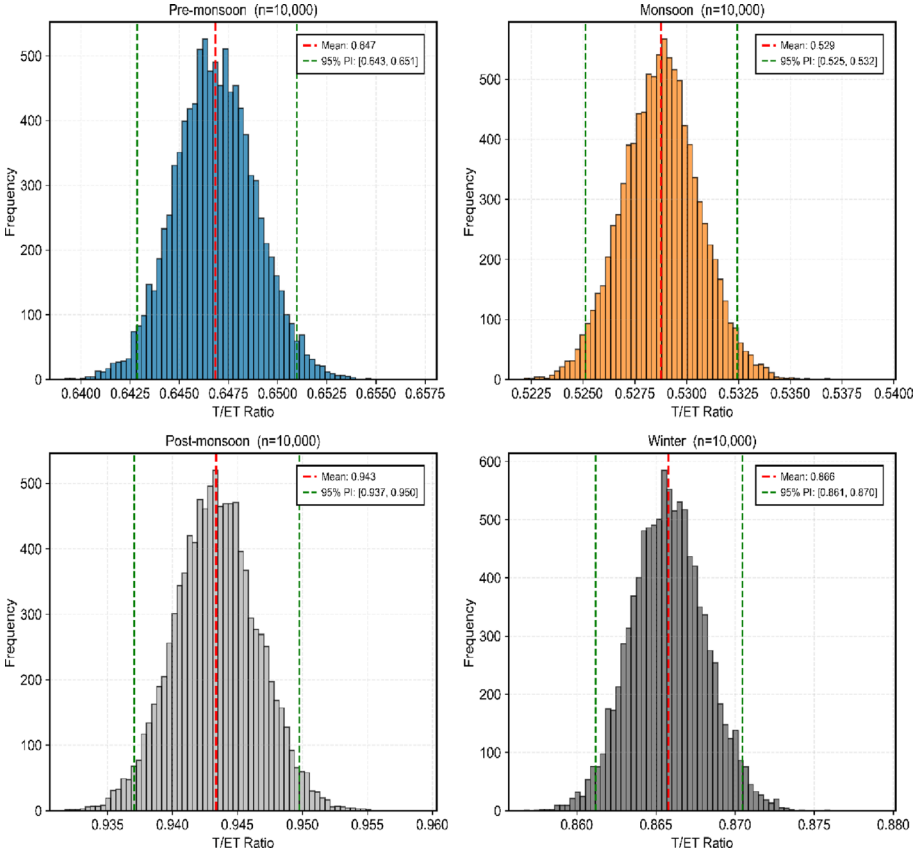


Fig. 6 Monte Carlo histograms by season

T/ET shows strong negative correlations with precipitation ($r = -0.72$) and minimum temperature ($r = -0.71$), implying that wetter conditions favour evaporation more than transpiration, thereby reducing the transpiration fraction of ET. In addition to soil saturation, persistent cloud cover during the monsoon likely also contributed to the observed decline in transpiration. As a C3 species sensitive to light availability, Syngonium podophyllum would be expected to show reduced stomatal conductance and photosynthetic activity under overcast conditions, reinforcing the suppression of transpiration driven by soil wetting.

Relative humidity exhibits a positive correlation with T/ET ($r = 0.37$), consistent with the idea that humid air reduces vapor pressure deficits and limits evaporation, allowing the transpiration share within ET to increase under moisture at −0.72 atmospheric conditions.

3.7.1 Temperature influence

All temperature metrics correlate negatively with T/ET, and the strongest effect is from minimum temperature, suggesting that higher nocturnal or cooler-range temperatures coincide with conditions that enhance non-stomatal losses relative to plant-controlled fluxes at this site. This pattern is consistent with the thermodynamic control whereby increased air temperature elevates atmospheric vapor-holding capacity and evaporative demand, often amplifying evaporation more directly than transpiration when moisture is available.

Table 6 Monte Carlo means, SD, 95% PI, and sensitivity weights

Season	Mean T/ET	SD	95% PI (lower)	95% PI (upper)	Sensitivity δ_{ET}(%)	Sensitivity E (%)	Sensitivity T (%)
Pre-monsoon	0.647	0.002	0.643	0.651	50.1	17.7	32.2
Monsoon	0.529	0.002	0.525	0.532	49.6	23.6	26.7
Post-monsoon	0.943	0.003	0.937	0.950	50.3	2.8	46.9
Winter	0.866	0.002	0.861	0.870	49.8	6.6	43.5

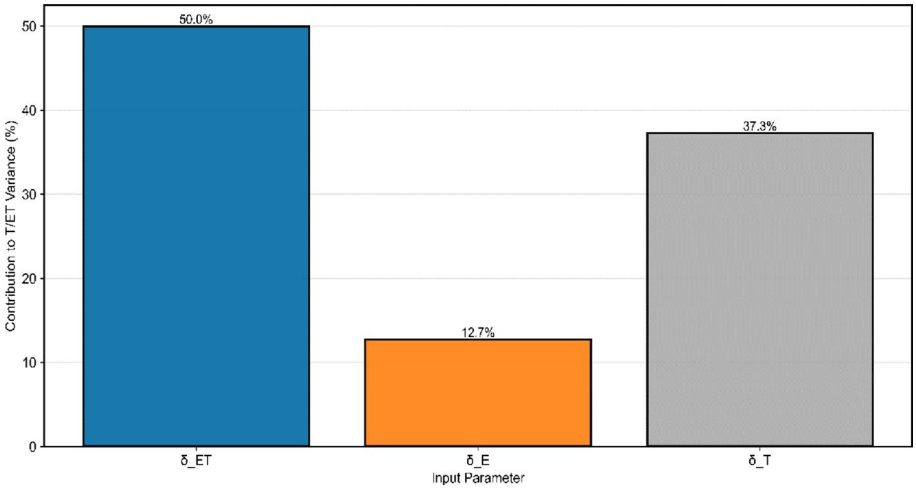


Fig. 7 Sensitivity analysis bar chart

3.7.2 Moisture variables

The strong inverse link between precipitation and T/ET indicates that rainfall events increase available surface water and soil wetness, thereby boosting evaporation and lowering the transpiration fraction within total ET during wet periods. In contrast, higher relative humidity is associated with higher T/ET, reflecting reduced aerodynamic and vapor pressure gradients that suppress evaporation and shift the balance toward plant-controlled transpiration under humid conditions.

3.7.3 Wind effects

Wind velocity shows a moderate negative correlation with T/ET ($r = -0.49$), supporting the role of wind in thinning the boundary layer and enhancing removal of water vapor, processes that typically accelerate evaporation more than plant-regulated transpiration. Although meaningful, wind's effect appears secondary to temperature and moisture controls in shaping the partitioning signal at the monthly scale represented here.

3.7.4 Evaporation response

Evaporation correlates strongly and negatively with T/ET ($r = -0.67$), consistent with evaporation's rapid, non-regulated response to meteorological forcing relative to the stomatal and physiological controls governing transpiration. This immediate coupling to atmospheric demand means increases in environmental drivers tend to raise total ET primarily via evaporation, thereby lowering the transpiration fraction.

3.7.5 Systemic and climatic implications

The predominance of negative correlations indicates that, under the observed conditions, meteorological variability tends to amplify evaporation more than transpiration, reducing T/ET and highlighting the need to represent aerodynamic and energy constraints in partitioning models. The positive role of relative humidity underscores the importance of atmospheric resistance and VPD-related processes, which many recent ET modelling and evaluation studies emphasize when projecting climate change impacts on regional water balances (Fig. 8).

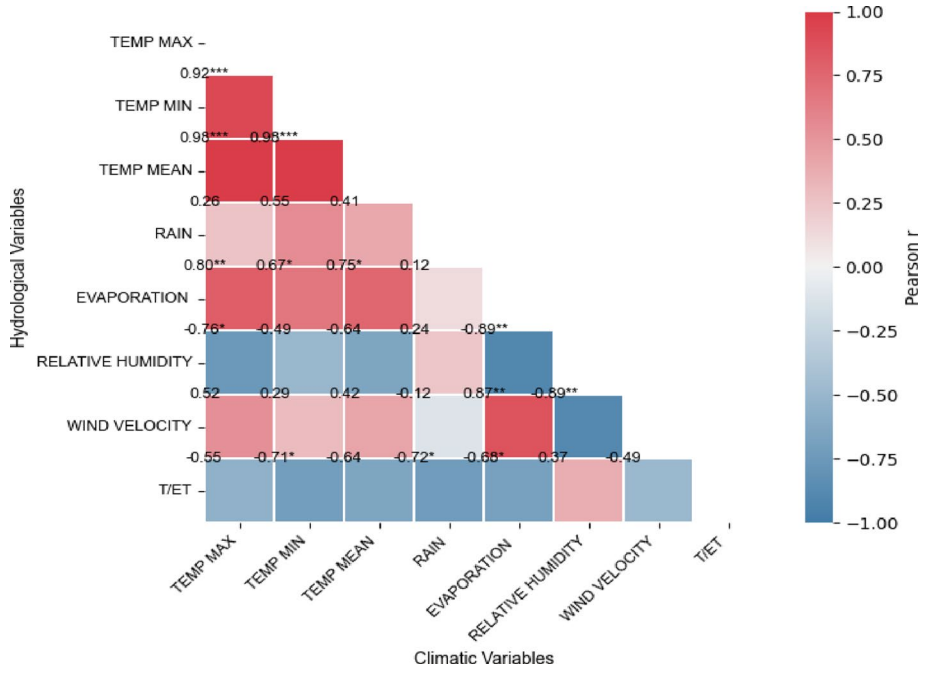


Fig. 8 Correlation matrix between T/ET and meteorological variables

4 Conclusion

This work advances an operational, isotope-informed framework for diagnosing seasonal shifts between evaporation- and transpiration-dominated regimes and translating those shifts into decisions that matter for water allocation and on-farm practice. By integrating vapor isotope Keeling analysis, partitioning with quantified uncertainty, and climate–partitioning linkages, the study provides defensible triggers for when to schedule or defer irrigation, where to prioritize canal lining and seepage control, and when to time managed aquifer recharge to minimize evaporative losses while supporting crop water productivity. The approach is immediately transferable to advisory systems because it relies on routinely observed meteorology coupled with a lean isotope program, and the uncertainty analysis specifies which measurements yield the largest gains in decision confidence. Limitations include potential site-specificity, event-scale variability that can be smoothed in monthly data, and drift in source end-members across crops and storms; addressing these will require spatial networks across soil–crop–groundwater settings, sub-daily campaigns through storms and heatwaves, and periodic end-member recalibration. Future work should embed these partitioning constraints in crop, groundwater, and river-operation models to test irrigation and recharge scenarios under warming monsoon climates, fuse remote sensing of canopy temperature and soil moisture to map field-scale transpiration efficiency, and co-develop farmer-facing rules of practice that are validated through on-farm trials tracking yield, water productivity, and salinity. Collectively, the framework turns isotopic diagnostics into actionable planning levers—reducing evaporative losses, stabilizing allocations, and improving equity and resilience of irrigation systems as hydroclimatic variability intensifies.

Supplementary Information

The online version contains supplementary material available at https://doi.org/10.1007/s44288-026-00782-1.

Supplementary Material 1.

Supplementary Material 2.

Author contributions
G.K. is responsible for the conceptualization of this manuscript, its planning and execution at NIH, A.C. preparing first and corrections draft, A.A. Reviewing and Editing, M.S.R experimentation part. S.T. conceptualization, methodology. P.S., D.B, R.O., R.S. and S.G. reviewed and edited the manuscript. All authors have worked as a team in planning its execution.

Funding
received from DST-SERB vide Sanction order: CRG/2020/004706 is duly acknowledged. Thanks to the anonymous reviewers for improving the quality of the manuscript.

Data availability
The datasets generated and/or analysed during the current study are available from the corresponding author upon reasonable request.

Declarations

Ethics approval and consent to participate
Not applicable, as this study did not involve human participants or animals.

Consent for publication
Not applicable, as no identifiable personal data or images are included in this manuscript

Competing interests
The authors declare no competing interests.

Received: 1 June 2026 / Accepted: 18 October 2026
Published online: 30 October 2026

References

1. Wang Z, Cao S, Cao G, Hou Y, Wang Y, Kang L. The Partitioning of Catchment Evapotranspiration Fluxes as Revealed by Stable Isotope Signals in the Alpine Inland River Basin. Water (Basel). 2022;14:790. https://doi.org/10.3390/w14050790.
2. Lu L, Zhang D, Zhang J, Zhang J, Zhang S, Bai Y, et al. Ecosystem Evapotranspiration Partitioning and Its Spatial–Temporal Variation Based on Eddy Covariance Observation and Machine Learning Method. Remote Sens (Basel). 2023;15:4831. https://doi.org/10.3390/rs15194831.
3. Peddinti SR, Kambhammettu P. Evapotranspiration partitioning in semi-arid agricultural systems using stable isotopes 2019;213:913–22.
4. Lu Y, Wen M, Li P, Liang J, Wei H, Li M. An Improved Craig–Gordon Isotopic Model: Accounting for Transpiration Effects on the Isotopic Composition of Residual Water during Evapotranspiration. Agronomy. 2023;13:1531. https://doi.org/10.3390/agronomy13061531.
5. Rothfuss Y, Quade M, Brüggemann N, Graf A, Vereecken H, Dubbert M. Reviews and syntheses: Gaining insights into evapotranspiration partitioning with novel isotopic monitoring methods. Biogeosciences. 2021;18:3701–32. https://doi.org/10.5194/bg-18-3701-2021.
6. Reich EG, Samuels-Crow K, Bradford JB, Litvak M, Schlaepfer DR, Ogle K. A Semi-Mechanistic Model for Partitioning Evapotranspiration Reveals Transpiration Dominates the Water Flux in Drylands. J Geophys Res Biogeosci. 2024;129. https://doi.org/10.1029/2023JG007914.
7. Sutanto SJ, Wenninger J, Coenders-Gerrits AMJ, Uhlenbrook S. Partitioning of evaporation into transpiration, soil evaporation and interception: a comparison between isotope measurements and a HYDRUS-1D model. Hydrol Earth Syst Sci. 2012;16:2605–16. https://doi.org/10.5194/hess-16-2605-2012.
8. Good SP, Noone D, Bowen G. Hydrologic connectivity constrains partitioning of global terrestrial water fluxes. Sci (1979). 2015;349:175–7. https://doi.org/10.1126/science.aaa5931.
9. Kulmatiski A, Forero LE, Bagging. A cheaper, faster, non-destructive transpiration water sampling method for tracer studies. Plant Soil. 2021;462:603–11.
10. Sun X, Wang L, Yakir D. Partitioning evapotranspiration with stable isotopes: Methods, uncertainties, and opportunities. Agric Meteorol 2021;307.
11. Ma Y, Song X. Seasonal variation of evapotranspiration partitioning and water use efficiency in a wheat–maize cropping system. Agric Water Manage. 2019;213:913–22.
12. Krishan G, Rao MS, Singh B, Sivapreeetha SVD, Thakur PK, Singh P, et al. Intra-annual variations in isotopic composition of atmospheric water vapour in a semi-arid monsoon region: observations and inferences. Discover Atmos. 2024;2:7. https://doi.org/10.1007/s44292-024-00010-w.
13. Rothfuss Y, Javaux M, Doussan C. Isotopic approaches to quantify root water uptake: A review and comparison of methods. Biogeosciences. 2010;7:1933–51.
14. Chakraborty S, Belekar AR, Datye A, Sinha N. Isotopic study of intraseasonal variations of plant transpiration: an alternative means to characterise the dry phases of monsoon. Sci Rep. 2018;8:8647. https://doi.org/10.1038/s41598-018-26965-6.
15. Menchaca LB, Smith BM, Connolly J, Conrad M, Emmett B. A method to determine plant water source using transpired water 2007. https://doi.org/10.5194/hessd-4-863-2007
16. Yakir D, Sternberg LdaSL. The use of stable isotopes to study ecosystem gas exchange. Oecologia. 2000;123:297–311. https://doi.org/10.1007/s004420051016.
17. Keeling CD. The concentration and isotopic abundances of carbon dioxide in the atmosphere. Tellus. 1958;10:174–93.

18. Lawrence DM, Thornton PE, Oleson KW, Bonan GB. The partitioning of evapotranspiration into transpiration, soil evaporation, and canopy evaporation in a GCM: Impacts on land–atmosphere interaction. J Hydrometeorol. 2007;8:862–80.
19. Xiao W, Wang L, Yakir D. Partitioning evapotranspiration using high-frequency stable water vapor isotope measurements. Agric Meteorol. 2018;252:327–41.
20. Good SP, Soderberg K, Wang L, Caylor KK, Coplen TB. $\delta^{18}O$ of water vapor in the vadose zone. Hydrol Earth Syst Sci. 2012;16:3465–78.
21. Craig H, Gordon LI. Deuterium and oxygen 18 variations in the ocean and the marine atmosphere. In: Tongiorgi E, editor. Stable Isotopes in Oceanographic Studies and Paleotemperatures. Spoleto: Consiglio Nazionale delle Ricerche, Laboratorio di Geologia Nucleare; 1965. pp. 9–130.
22. Lyu S, Wang J. Transpiration Induced Changes in Atmospheric Water Vapor δ18O via Isotopic Non-Steady-State Effects on a Subtropical Forest Plantation. Water (Basel). 2022;14:2648. https://doi.org/10.3390/w14172648.
23. Fiorella RP, West JB, Bowen GJ. Biased estimates of the isotope ratios of steady-state evaporation from the assumption of equilibrium between vapour and precipitation. Hydrol Process. 2019;33:2576–90. https://doi.org/10.1002/hyp.13531.
24. Yao T, Zhang X, Guan H, Zhou H, Hua M, Wang X. Climatic and environmental controls on stable isotopes in atmospheric water vapor near the surface observed in Changsha, China. Atmos Environ. 2018;189:252–63. https://doi.org/10.1016/j.atmosenv.2018.07.008.
25. Coplen TB. New guidelines for reporting stable hydrogen, carbon, and oxygen isotope-ratio data. Geochim Cosmochim Acta. 1996;60:3359–60. https://doi.org/10.1016/0016-7037(96)00263-3.
26. Wang XF, Yakir D. Using stable isotopes of water in evapotranspiration studies. Hydrol Process. 2000;14:1407–21.
27. Uddin MG, Nash S, Rahman A, Olbert AI. A novel approach for estimating and predicting uncertainty in water quality index model using machine learning approaches. Water Res. 2023;229:119422. https://doi.org/10.1016/j.watres.2022.119422.
28. Zhou S, Yu B, Zhang Y, Huang Y, Wang G. Water use efficiency and evapotranspiration partitioning for three typical ecosystems in the Heihe River Basin, northwestern China. Agric Meteorol. 2018;253–254:261–73. https://doi.org/10.1016/j.agrformet.2018.02.002.
29. Cohen J. Statistical Power Analysis for the Behavioral Sciences. Routledge; 2013. https://doi.org/10.4324/9780203771587.
30. Agbangba CE, Sacla Aide E, Honfo H, Glèlè Kakai R. On the use of post-hoc tests in environmental and biological sciences: A critical review. Heliyon. 2024;10:e25131. https://doi.org/10.1016/j.heliyon.2024.e25131.
31. Johnson DL, Statistical methods for occupational, exposure assessment. Handbook of Occupational Safety and Health. Wiley; 2019. pp. 125–45. https://doi.org/10.1002/9781119581482.ch5.
32. Saranya P, Krishnakumar A, Sinha N, Kumar S, Anoop Krishnan K. Isotopic signatures of moisture recycling and evaporation processes along the Western Ghats orography. Atmos Res. 2021;264:105863. https://doi.org/10.1016/j.atmosres.2021.105863.
33. Müller T, Fischer M, Lane SN, Schaefli B. Separating snow and ice melt using water stable isotopes and glacio-hydrological modelling: towards improving the application of isotope analyses in highly glacierized catchments. Cryosphere. 2025;19:423–58. https://doi.org/10.5194/tc-19-423-2025.
34. Benettin P, Nehemy MF, Cernusak LA, Kahmen A, McDonnell JJ. On the use of leaf water to determine plant water source: A proof of concept. Hydrol Process. 2021;35. https://doi.org/10.1002/hyp.14073.
35. Gui Y, Wang K, Jin Z, Wang H, Deng H, Li X, et al. The decline in tropical land carbon sink drove high atmospheric CO2 growth rate in 2023. Natl Sci Rev. 2024;11. https://doi.org/10.1093/nsr/nwae365.
36. Ellsworth PZ, Williams DG. Hydrogen isotope fractionation during water uptake by woody xerophytes. Plant Soil. 2007;291:93–107. https://doi.org/10.1007/s11104-006-9177-1.
37. Hu S, Li Y, Chang SX, Li Y, Yang W, Fu W, et al. Soil autotrophic and heterotrophic respiration respond differently to land-use change and variations in environmental factors. Agric Meteorol. 2018;250–251:290–8. https://doi.org/10.1016/j.agrformet.2018.01.003.

Publisher's Note

Springer Nature remains neutral with regard to jurisdictional claims in published maps and institutional affiliations.